Early diagenetic siderite in the Panorama Point Beds (Radok Conglomerate, Early to Middle Permian), Prince Charles Mountains, East Antarctica

Krzysztof P. KRAJEWSKI [1,3*], Nikolai A. GONZHUROV [2], Anatoly A. LAIBA [2]
and Andrzej TATUR [3]

[1] *Instytut Nauk Geologicznych PAN, Twarda 51/55, 00-818 Warszawa, Poland*
*<kpkraj@twarda.pan.pl> *corresponding author*

[2] *Polar Marine Geological Research Expedition, Pobedy 24, 198412 St. Petersburg, Russia*

[3] *Zakład Biologii Antarktyki PAN, Ustrzycka 10/12, 02-141 Warszawa, Poland*

Abstract: The Panorama Point Beds represent a subfacies of the Early to Middle Permian Radok Conglomerate, which is the oldest known sedimentary unit in the Prince Charles Mountains, MacRobertson Land, East Antarctica. This unit records clastic sedimentation in fresh-water depositional system during the early stages of development of the Lambert Graben, a major structural valley surrounded by crystalline highlands in the southern part of Gondwana. It contains common siderite precipitated through early diagenetic processes in the swamp, stagnant water, and stream-flow environments. There are two types of siderite in the Panorama Point Beds: (1) disseminated cement that occurs throughout the sedimentary succession; and (2) concretions that occur at recurrent horizons in fine-grained sediments. The cement is composed of Fe-depleted siderite (less than 90 mol % $FeCO_3$) with an elevated content of magnesium, and trace and rare earth elements. It has negative $\delta^{13}C_{VPDB}$ values (-4.5 to -1.5‰). The concretions are dominated by Fe-rich siderite (more than 90 mol % $FeCO_3$), with positive $\delta^{13}C_{VPDB}$ values (+1 to +8‰). There are no noticeable differences in the oxygen ($\delta^{18}O_{VPDB}$ between -20 and -15‰) and strontium ($^{87}Sr/^{86}Sr$ between 0.7271 and 0.7281) isotopic compositions between the siderite types. The cement and concretions developed in the nearsurface to subsurface environment dominated by suboxic and anoxic methanic degradation of organic matter, respectively. The common presence of siderite in the Panorama Point Beds suggests that fresh-water environments of the Lambert Graben were covered by vegetation, starting from the early history of its development in the Early Permian.

Key words: Antarctica, Prince Charles Mts, Radok Conglomerate, Permian, siderite, fresh-water environment.

Introduction

Authigenic carbonate minerals in the late Paleozoic continental Gondwana sequences provide important data for interpreting the evolution of the environment, including climate, vegetation, water system, and nearsurface biogeochemical pro-

cesses (Gould and Smith 1979; Dickmann and Wopfner 1996; Mishira 1996; Yemane and Kelts 1996; Faure and Cole 1999; Uysal *et al.* 2000; Ketzer *et al.* 2003). They aid understanding of the geological history of Gondwanan glaciation, in particular the evolution of post-glacial environments, in which carbonate cements resulting from diagenetic transformations of sedimentary organic matter provide the first evidence of vegetation. The study of carbonate cements may therefore be helpful in discriminating between environments devoid of and covered by vegetation, which is usually difficult to decipher based on sedimentological investigations (dos Santos *et al.* 1996; Isbell *et al.* 2001).

This paper presents detailed analysis of siderite cement and concretions occurring in the Permian Radok Conglomerate (Prince Charles Mts, MacRobertson Land), the oldest recognized late Paleozoic sedimentary unit on the East Antarctic craton. These mineral deposits record suboxic to anoxic methanic degradation of organic matter in fresh-water environments of the southern continental Gondwana.

Geological setting

The East Antarctic Craton (Fig. 1) contains only one substantial outcrop of the late Paleozoic continental deposits, and this is located in the Amery Oasis in the northern Prince Charles Mountains, MacRobertson Land (Figs 2, 3). They are assigned to the Amery Group (Mond 1972), and comprise dominantly arkoses and
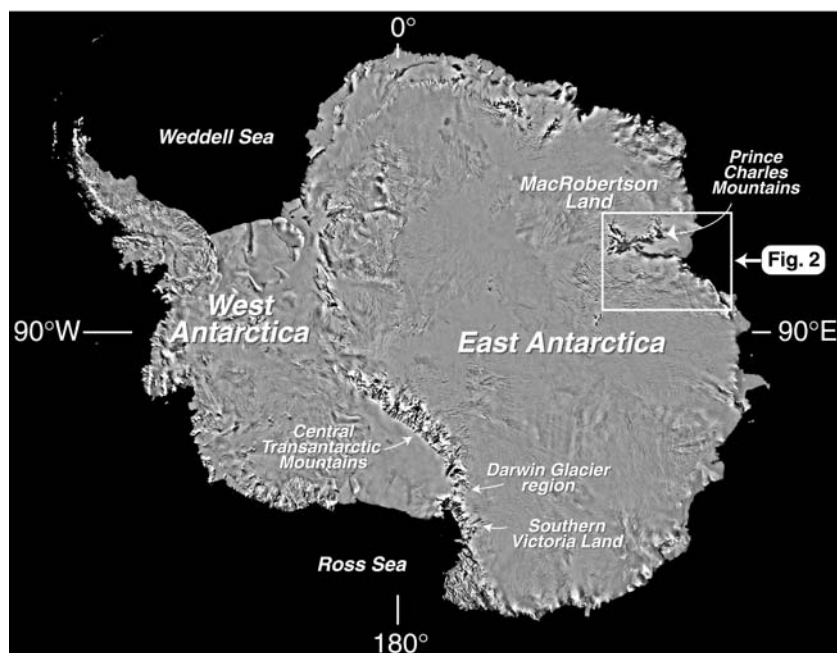

Fig. 1. Map of Antarctica showing crucial locations of the late Paleozoic sedimentary exposures.
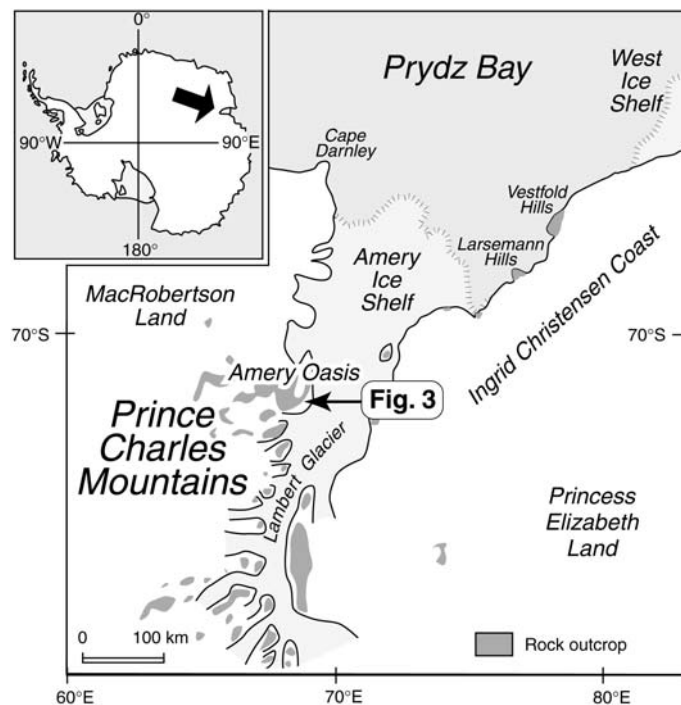
Fig. 2. Map of the MacRobertson Land – Princess Elizabeth Land area in East Antarctica showing location of the Amery Oasis in the Prince Charles Mountains.
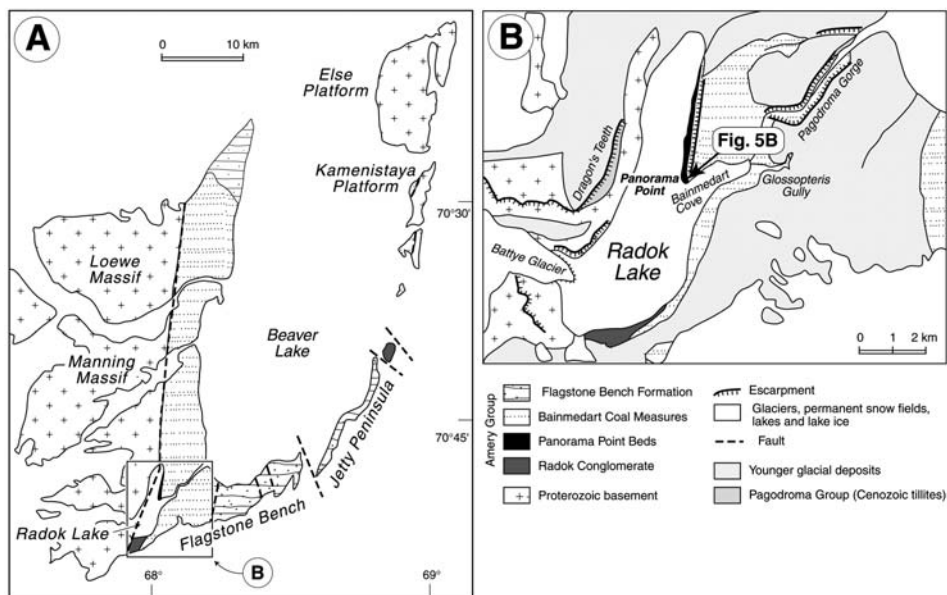

Fig. 3. Geological maps of the Amery Oasis (**A**) and the Radok Lake area (**B**) showing outcrops of the Radok Conglomerate and location of section of the Panorama Point Beds analyzed in this paper.
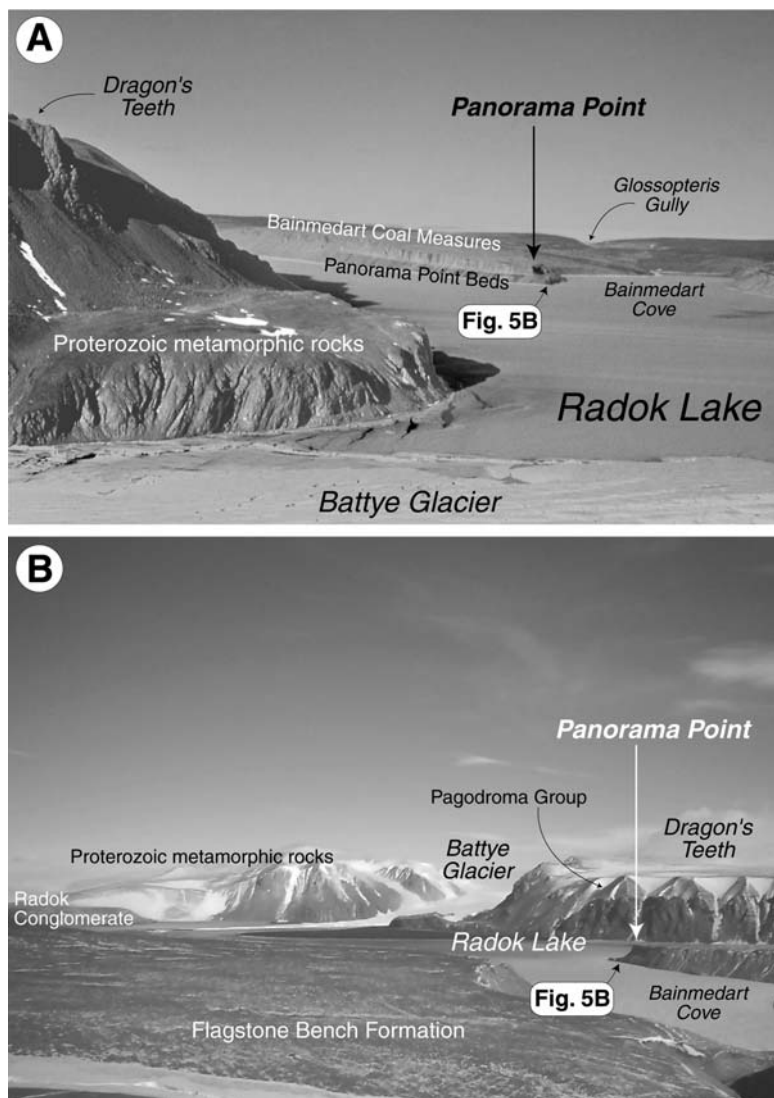
Fig. 4. Panorama Point at the northeastern coast of Radok Lake seen from the west (**A**) and from the east (**B**). For stratigraphy of the rocks exposed see Fig. 5.

subarkoses, with subordinate conglomerates, siltstones, mudstones, shales, and coals (Ravich 1974; Aleksashin and Laiba 1993). Palynomorphs and plant fossils indicate a Permo-Triassic age for the succession (White 1969; Dibner 1976; Webb and Fielding 1993a; Cantrill *et al.* 1995; McLoughlin and Drinnan 1997a, b; McLoughlin *et al.* 1997; Lindström and McLoughlin 2007).

The Amery Group (Figs 4, 5) is subdivided into three formations (in ascending order): the Radok Conglomerate, the Bainmedart Coal Measures, and the Flagstone Bench Formation (McLoughlin and Drinnan 1997a, b). It was deposited by a
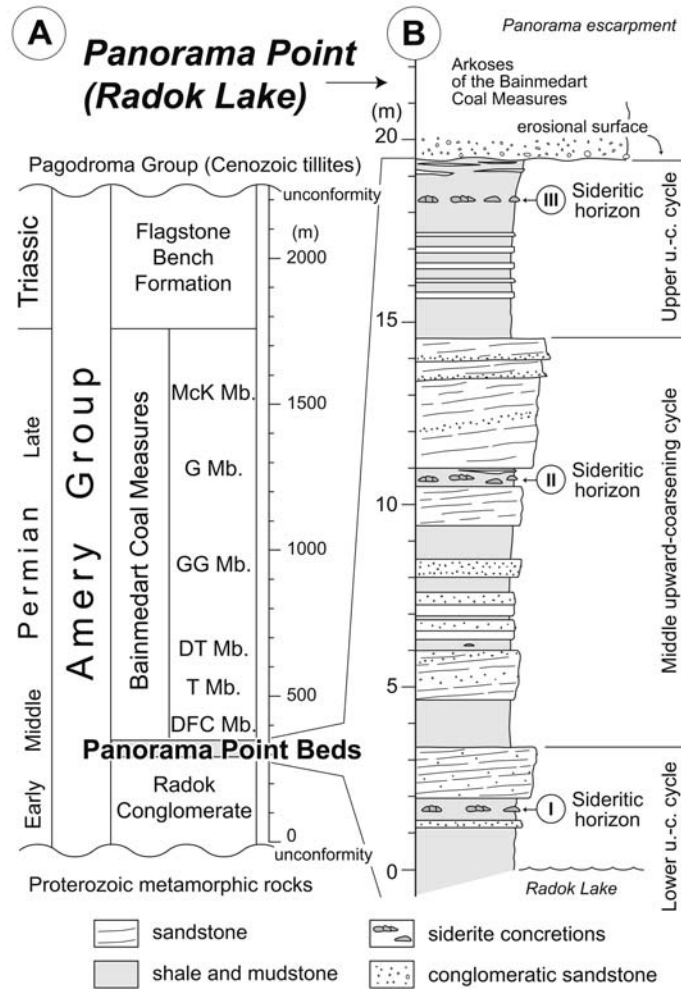
Fig. 5. **A**. Stratigraphic subdivision of the Amery Group in the Prince Charles Mountains (after McLoughlin and Drinnan 1997a, b and Mikhalsky *et al.* 2001). **B**. Detailed section of the Panorama Point Beds at Panorama Point. DFC Mb. – Dart Fields Conglomerate Member; T Mb. – Toploje Member; DT Mb. – Dragons Teeth Member; GG Mb. – Glossopteris Gully Member; G Mb. – Graingner Member; McK Mb. – McKinnon Member.

low sinuosity braided river system flowing axially northwards along the Lambert Graben, a major structural valley in this part of Gondwana (McKelvy and Stephenson 1990; Webb and Fielding 1993b; Fielding and Webb 1966). The graben is interpreted to be a continental rift valley, formed by limited crustal extension (Fedorov *et al.* 1982; Harrowfield *et al.* 2005). Superposition of red-bed sediments (Flagstone Bench Formation – Triassic part of the Amery Group) on coal-bearing clastic strata (Bainmedart Coal Measures – Middle to Late Permian) and conglomeratic sequences (Radok Conglomerate – Early to Middle Permian) records a gen-
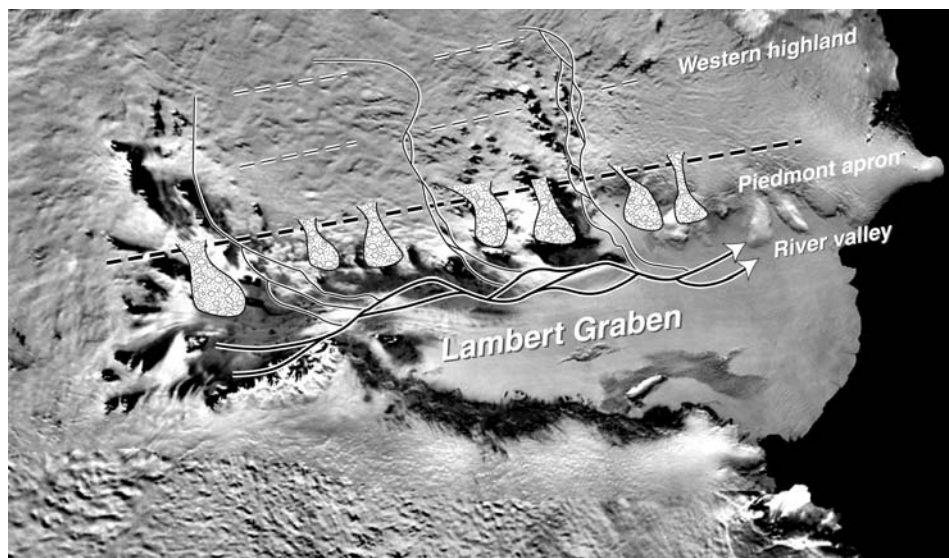
Fig. 6. Paleoenvironmental interpretation and paleogeography of the Radok Conglomerate superimposed on satellite photo of the Lambert Glacier – Prince Charles Mountains – Amery Ice Shelf area. Reconstruction after Fielding and Webb (1995), slightly modified.

eral climatic change from cold and temperate wet climate towards a drier and warmer one, but returning again to wetter conditions in the Late Triassic (Cantrill *et al.* 1995; McLoughlin *et al.* 1997). However, there are no signs of glacial conditions at base of the succession (Mikhalsky *et al*. 2001). A large Gondwanan glaciation in Carboniferous and Early Permian covering the East Antarctic craton (including the study area) is commonly accepted in the literature (Scotese 1997; Zeigler *et al.* 1997; Scotese *et al.* 1999).

The Radok Conglomerate provides the oldest sedimentary record in the region. The published spore and pollen assemblages have been interpreted to be Early to Middle Permian in age (Kemp 1973; Ravich 1974; Dibner 1978; Lindström and McLoughlin 2007). The Radok Conglomerate comprises an upward-fining succession, starting with coarse conglomerates and breccias composed of pebbles, boulders and debris derived from local Proterozoic basement. These sediments pass upwards into immature arkoses and subarkoses interfingered with conglomeratic sandstones and relatively fine conglomerates. Sedimentary features suggest deposition in a coarse alluvial fan forming a piedmont apron, during a period of intense faulting associated with the onset of the Lambert Graben formation (McKeley and Stephenson 1990; Fielding and Webb 1995; Mikhalsky *et al*. 2001). The Radok Conglomerate is interpreted to have formed principally by eastward sediment supply into the western part of the Lambert Graben, transverse to its structural axis (Fig. 6). The western part of the Lambert Graben, termed the Beaver Lake Graben (or sub-basin), is separated from the main graben structure by the
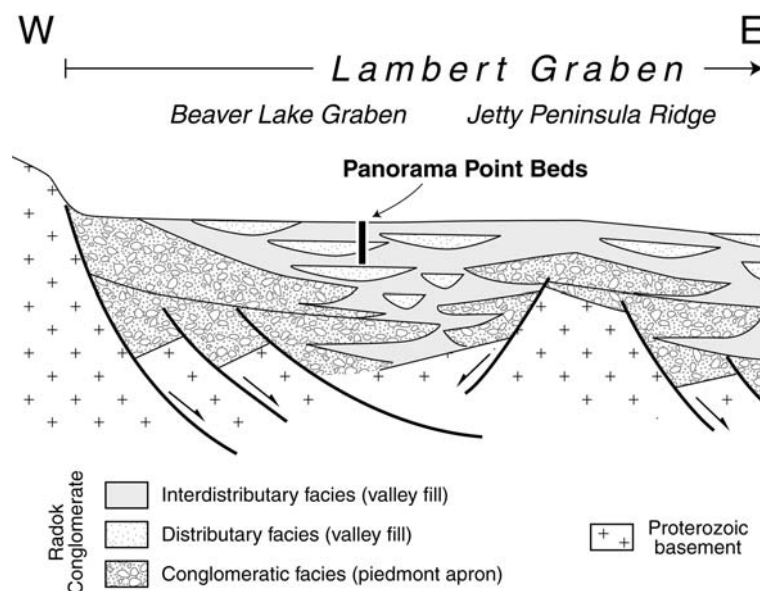
Fig. 7. Conceptual section of the Radok Conglomerate across the Beaver Lake Graben and Jetty Peninsula Ridge (eastern part of the Lambert Graben) showing facies position of the Panorama Point Beds.

Jetty Peninsula Ridge (Fig. 7). It formed as a structural component of the rift system, and preserves a well-exposed record of the early history of the graben filling. A general fining-upward trend observed in the Radok Conglomerate suggests that sediment supply to the basin margin apron gradually receded, most probably as a result of progressive weathering and erosion of the adjacent highland. This decline in transverse sediment supply, coupled with the progressive filling of extensional graben topography, allowed increasing avulsion of axially flowing streams (northwards) sourced from the south. The lateral extent of sedimentation has progressively increased through time, transforming from coarse-grained apron(s) and alluvial fans to broad valley with braided rivers and deltas.

The upper part of the Radok Conglomerate, termed the Panorama Point Beds (McKelvey and Stephenson 1990), consists of medium-grained sandstones intercalated with conglomeratic sandstones and dark mudstones-shales that are arranged in three superimposed upward-coarsening cycles (Fig. 5B). They represent delta-front sediments deposited in flowing and shallow stagnant water surrounded by swamps and wetlands (Fig. 7). The lower and middle cycles are more or less completely preserved, whereas the upper one is variably cut by an erosional surface that constitutes the base of the overlying arkoses of the Bainmedart Coal Measures. This suggests subtle synsedimentary re-structuring of the graben associated with the activity of normal faults (Fielding and Webb 1995). A discontinuous, but laterally extensive, thin conglomerate unit covering the erosional surface is distinguished as the Dart Fields Conglomerate Member of the Bainmedart Coal Mea-

sures (McKelvey and Stephenson 1990; McLoughlin and Drinnan 1997a, b; Mikhalsky *et al*. 2001).

The Panorama Point Beds constitute a facies variant of the upper Radok Conglomerate, which is preserved mostly on the northeastern shores of Radok Lake (Figs 3, 4). Fine-grained sediments of the Panorama Point Beds contain carbonized plant debris and palynomorphs. Siderite cement is common throughout the unit, and there are three distinct horizons of siderite concretions in shaly intervals, one in each of the cycles (Fig. 5B). It is the oldest confirmed occurrence of early diagenetic carbonate precipitate in the Amery Group. Siderite concretions become more common in the Dragons Teeth Member of the Bainmedart Coal Measures, where they occur in lacustrine settings in horizons enriched in plant fragments (Fielding and Webb 1996).

Materials and methods

The present study is based on a section through the Panorama Point Beds located at Panorama Point on the northeastern coast of Radok Lake (Figs 3, 4). This section corresponds to Section I of Fielding and Webb (1995). It embraces the upper part of the lower cycle, the whole middle cycle, and the upper cycle up to its erosional surface with the overlying arkoses of the Bainmedart Coal Measures (Fig. 5). The unit is exposed on the rocky slope that emerges above the level of Radok Lake, extending up to the foot of a steep cliff formed by the overlying arkoses.

Forty samples of siderite concretions and the host rock were collected through the section. Seven, seven, and nine concretions were taken from the I, II, and III sideritic horizons, respectively. Two, six, and seven samples of the host rock were taken from the I, II, and III upward-coarsening cycles, respectively. Classification of detrital rocks after Folk (1974) was followed for the description of discerned lithologies.

All samples were analyzed using standard petrographic methods, including transmitted (TLM) and reflected light mcroscopy (RLM), back-scattered electron imaging (BSE), and energy-dispersive X-ray spectroscopy (EDS). BSE images were obtained using a JEOL JSM-840A scanning electron microscope operating at 15kV acceleration voltage. Quantitative EDS analyses of siderite were obtained using the same microscope, equipped with a THERMO NORAN VANTAGE EDS system. Operating conditions were a 15 kV acceleration voltage, 1 to 5 mm beam diameter, and 100 s counting time. Detection limits of the analyzed elements (Ca, Mg, Fe, Mn) were better than 0.05 wt. %. To facilitate comparison among samples, the EDS data were recalculated as cation mol fractions.

Mineral compositions of the host rock and siderite concretions were analyzed by means of X-ray diffraction (XRD). Samples were ground to <63 μm fraction.

Diffraction patterns were recorded on a SIGMA 2070 diffractometer using a curved position sensitive detector in the range 2–120° 2θ with CoKα radiation and 20 hour analysis time. DIFFRACTIONEL software v. 03/93 was used to process the obtained data.

The samples were analyzed for the carbon and oxygen isotopic composition of siderite. CO_2 for isotopic analyses was produced from samples by reaction with anhydrous phosphoric acid (d = 1.90 g cm^{-3}) at 50°C over 120 h. Isotopic $^{13}C/^{12}C$ and $^{18}O/^{16}O$ ratios were determined using a FINNIGAN MAT DELTA^{PLUS} spectrometer working in dual inlet mode with universal triple collector. The results are expressed as $\delta^{13}C$ and $\delta^{18}O$ notations with respect to VPDB. The acid fractionation factor for oxygen in siderite at 50°C $\alpha_{(CO2-FeCO3)}$ = 1.01079 (Carothers $et\ al.$ 1988) was used. Analytical reproducibility was better than ± 0.05‰ and ± 0.1‰ for $\delta^{13}C$ and $\delta^{18}O$, respectively.

The content of trace and rare earth elements was analysed in selected samples using ICP-MS and ICP-ES methods at ACME Analytical Laboratories. Three samples of concretions (S1, S2, and S3) and three samples of the host rock (H1, H2, and H3), representing the three discerned sideritic horizons, were analyzed. The same samples were analyzed for the strontium isotopic composition in siderite. A standard procedure of sample preparation was applied, and the $^{87}Sr/^{86}Sr$ isotopic ratio was determined using a Fisons thermoionization mass spectrometer (TIMS) VG SECTOR 54 equipped with eight collectors.

Results

Facies development and petrography of the clastic succession. — The coarsening-upward cycles of the Panorama Point Beds consist of clastic rocks that vary from mudstone to conglomeratic sandstone (Fig. 5B). Fine-grained intervals of the cycles comprise mud-shale that is variably sandy, and contains recurrent siltstone to sandstone beds. The mud-shale partings are rich in plant debris, with rooted zones (including *Vertebraria*) observed at some levels. The interbedded siltstones and sandstones show planar and ripple-cross-lamination to cross-bedding. This facies is interpreted to have been deposited in a swamp environment with stagnant water bodies (lakes and ponds) and local unconfined water flows in a distal alluvial fan setting. Coarse-grained intervals of the cycles occur in the form of sets of thick sandstone beds with erosive bases that are commonly conglomeratic and show dominant cross-bedding. They are dominated by quartz, feldspar, and grains of felsic granulite and felsic gneiss, the latter being the dominant lithologies of the Proterozoic basement in the area. The sandstones show wide variations in sorting and composition, suggesting contrasting transport from both local (transverse) and remote (axial) sources in the Lambert Graben. They are in-

terpreted to represent deposits of fan distributary channels that cut into inter-channel distal fan facies dominated by transient mire and stagnant water deposits.

Petrography of siderite. — Siderite in the Panorama Point Beds occurs in the form of: (1) concretions; and (2) disseminated cement in host rocks (Fig. 8).

The concretions concentrate in conspicuous horizons in the sequence (Fig. 9). They have a variety of shapes, including spherical, sub-spherical, cylindrical, flat, and composite that combine these forms in various geometric arrangements. Despite the morphologic variations, the concretions invariably show compact internal structure and warping of lamination around concretionary bodies, suggesting their early, syngenetic formation. All the observed concretions represent a
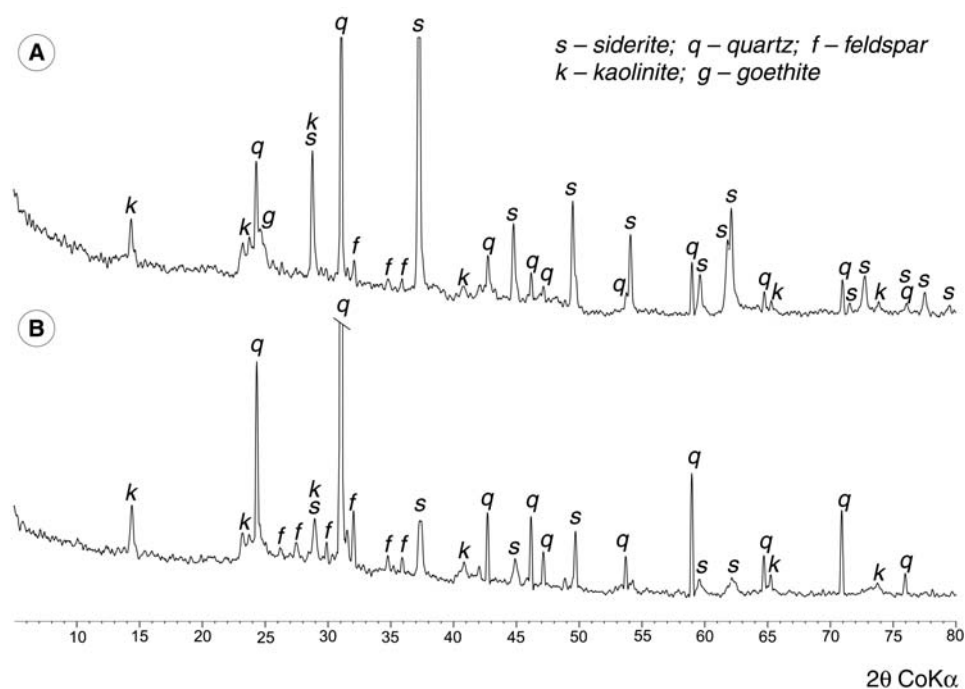
Fig. 8. X-ray diffraction patterns of siderite concretion (**A**) and the host sandy mud-shale (**B**). I sideritic horizon.
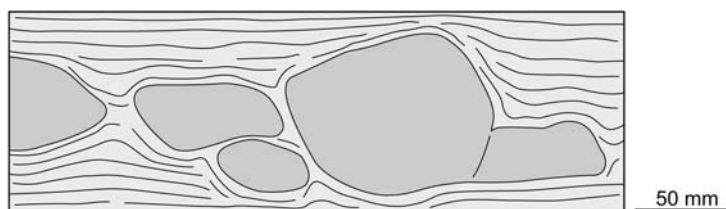
Fig. 9. Horizon of siderite concretions (I) in sideritic mud-shale of the Panorama Point Beds showing warping of lamination around the concretionary bodies. Field drawing.
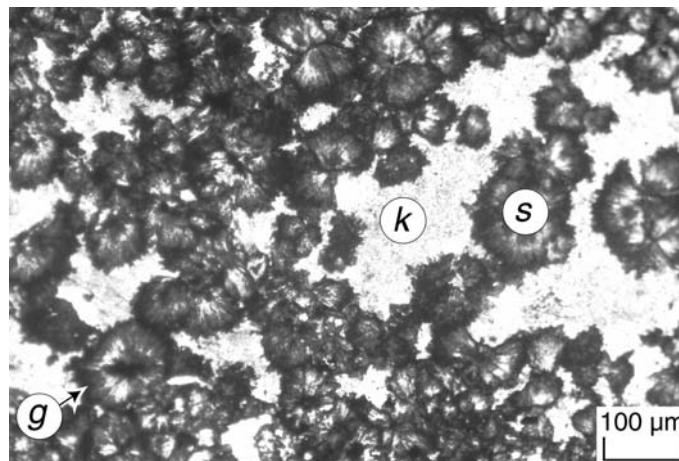
Fig. 10. Matrix of concretion showing aggregates of siderite spherules (s) with goethitic coatings (g). The remaining pore space is replaced by kaolinite cement (k). TLM photomicrograph, normal light.

pristine variety, *i.e.* they occur at their original growth position in sediment, without traces of subsequent reworking or other dynamic concentration processes. The sections of concretions show an uncompacted texture of relict sediment throughout the concretionary bodies. The exception is the very margins of concretions contacting the host rock, where the sediment shows compactional features. The concretions consist of a massive matrix dominated by microscopic siderite spherules, commonly with radial-fibrous internal structure (Figs 10, 11A, B). Locally these spherules have oxidized margins, accentuated by thin rims composed of goethite. The pore space between spherules is replaced mostly by diagenetic kaolinite cement. Microgranular pyrite is an accessory component, always embedded inside the spherules (Fig. 11C).

The host rocks in the concretionary horizons and most of the sediments elsewhere in the Panorama Point Beds show common siderite cement (Fig. 11D–F). This cement occurs in the form of disseminated microscopic clusters and coatings of detrital sediment grains. The volume of the cement varies from rare clusters in inter-particle pore space to abundant aggregates of clusters filling most of the pore space. Only in a few cases do the clusters show radial-fibrous internal structure.

Major element geochemistry of siderite. —Mean composition of siderite occurring in the form of concretions and in the form of disseminated cement in the I, II, and III sideritic horizons is:

(1) $Fe_{0.91}Mg_{0.05}Ca_{0.02}Mn_{0.02}CO_3 - Fe_{0.86}Mg_{0.10}Ca_{0.02}Mn_{0.02}CO_3$,

(2) $Fe_{0.91}Mg_{0.04}Ca_{0.03}Mn_{0.02}CO_3 - Fe_{0.87}Mg_{0.09}Ca_{0.01}Mn_{0.03}CO_3$,

(3) $Fe_{0.93}Mg_{0.03}Ca_{0.02}Mn_{0.02}CO_3 - Fe_{0.81}Mg_{0.08}Ca_{0.02}Mn_{0.09}CO_3$,
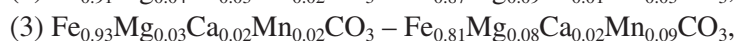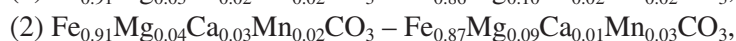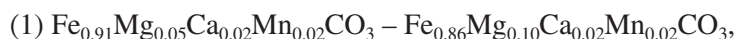
respectively (source data are listed on-line under the address http://www.polish.polar.pan.pl/SOM/PPR31-Krajewski.pdf). The disseminated siderite cement is
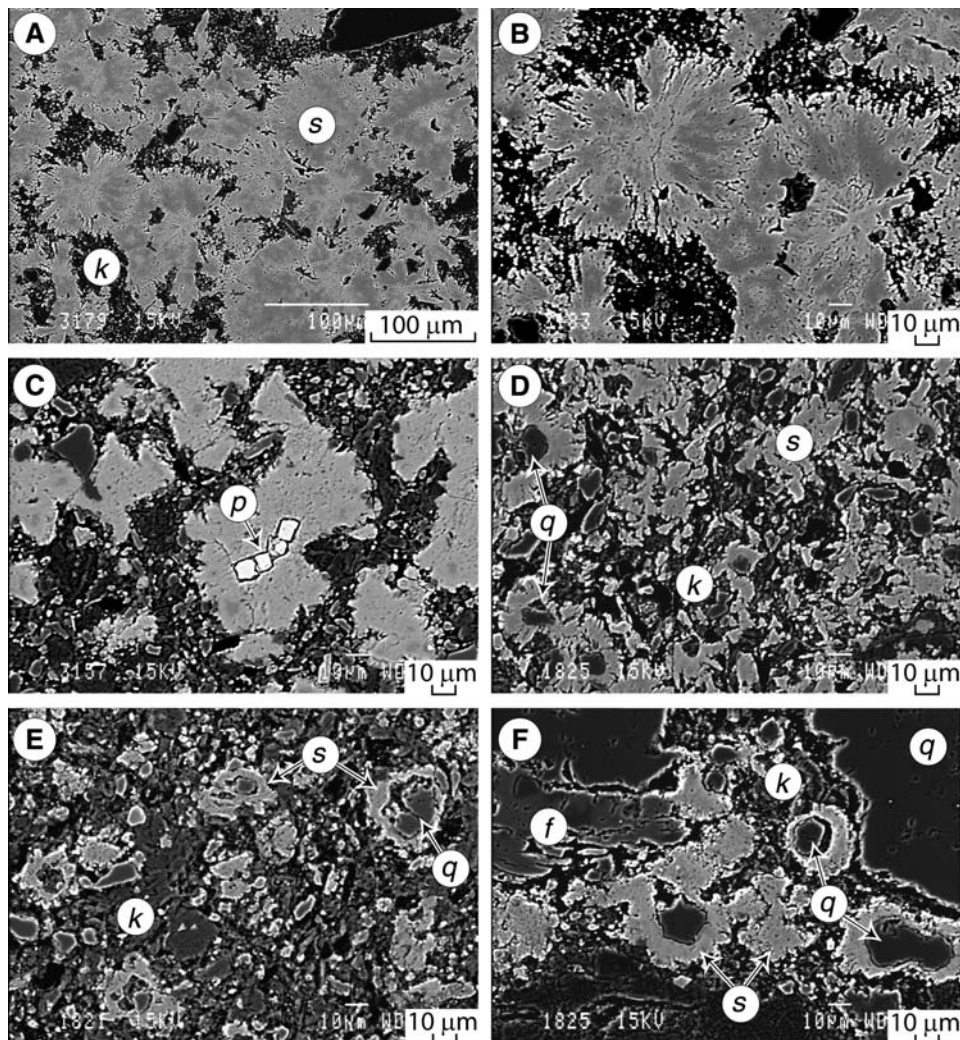
Fig. 11. **A**. Spherulitic siderite (s) forming matrix of a concretion. The remaining pore space is replaced by kaolinite cement (k). **B**. Radial-fibrous microstructure of siderite spherules. **C**. Microgranular pyrite (p) occurring in the centre of siderite spherule. **D**. Disseminated siderite clusters (s) in the mudstone matrix. Some siderite forms coatings around detrital quartz grains (q). Kaolinite (k) dominates the remainder of the rock matrix. **E**. Disseminated siderite clusters (s) in the siltstone matrix. Some of the siderite forms coatings around detrital quartz grains (q). Kaolinite (k) occurs in the matrix. **F**. Siderite clusters and coatings (s) of fine detrital grains in inter-particle pore space of sandstone bed. The detrital grains are dominated by quartz (q) and feldspar (f). The remaining pore space is replaced by kaolinite cement (k). A–F – BEI images of thin sections.

depleted in iron and enriched in magnesium, compared to siderite in concretions (Fig. 12). Calcium is an accessory component, though its content is roughly constant. This is also the case for manganese, except for the siderite cement in the upper upward-coarsening cycle, which is noticeably enriched in Mn.
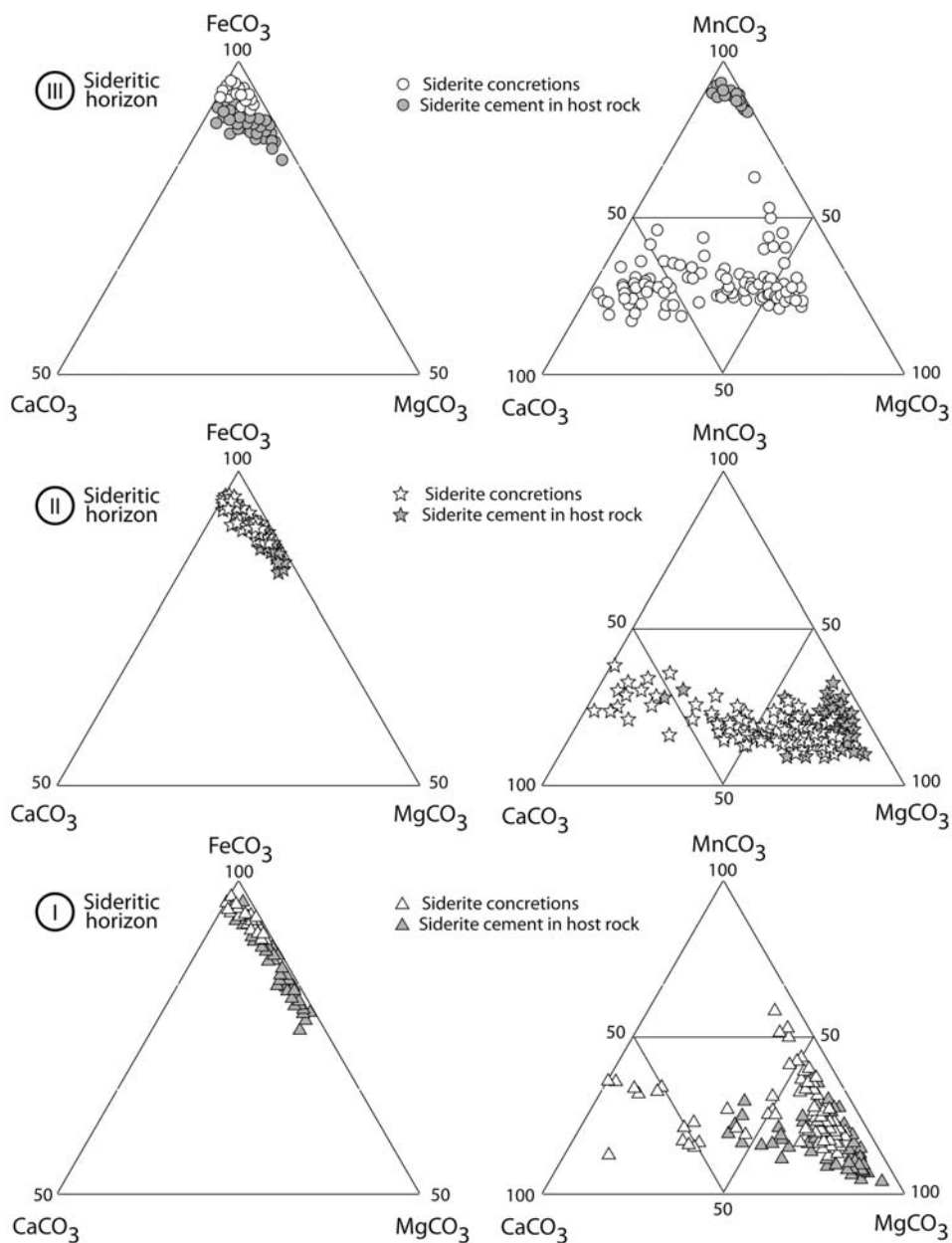
Fig. 12. Ternary diagrams illustrating chemical composition of siderite in concretions and in dissemi-nated cement in the I, II, and III sideritic horizons. Relative mol percentages of $FeCO_3$, $MgCO_3$, and $CaCO_3$ in diagrams on the left were recalculated for $MnCO_3 = 0\%$. Source data are listed on-line un-der the address http://www.polish.polar.pan.pl/SOM/PPR31-Krajewski.pdf.

On a microscale, the concretions show two distinct chemical compositions of siderite: (1) the Fe-rich variety, containing more than 90 mol % $FeCO_3$; and (2) the
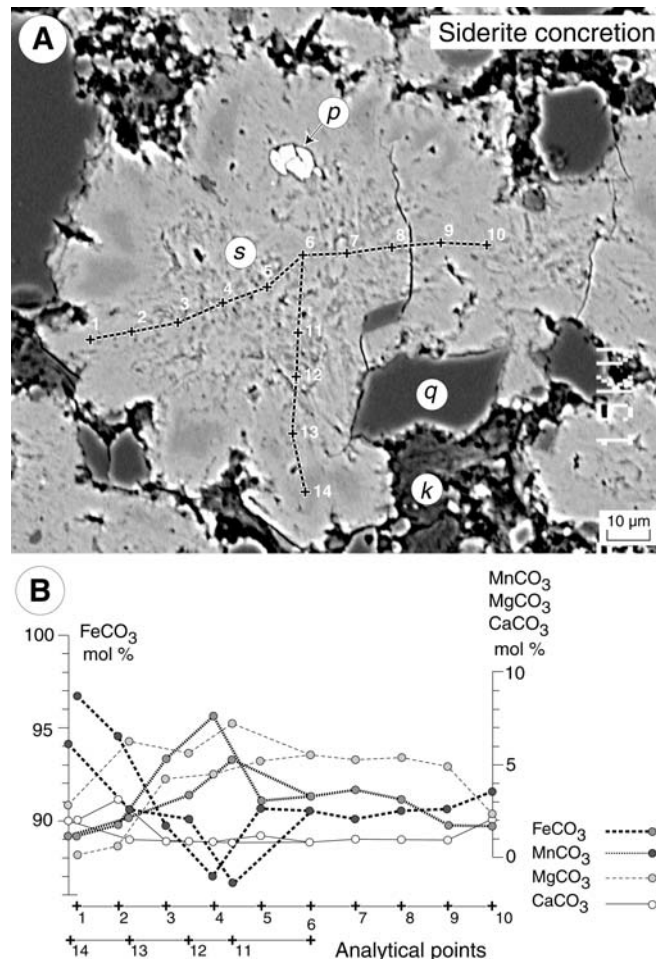
Fig. 13. Compositional changes in spherulitic siderite forming concretions in the sideritic horizon I. BEI image (**A**) of siderite spherule (s) embedding microgranular pyrite (p) and detrital quartz grains (g). Kaolinite (k) occurs in inter-particle pore space. 1 to 14 are analytical points along EDS quantitative compositional profile shown in **B**.

Fe-depleted variety, containing less than 90 mol % $FeCO_3$, and correspondingly more $MgCO_3$, and at places also $MnCO_3$. These two varieties tend to form external and internal parts of the siderite spherules, respectively (Figs 13, 14). However, detailed chemical trends in the spherules are complex and variable, reflecting presumably recrystallizational modifications associated with the development of their radial-fibrous structure. Disseminated siderite cement in the host rock is represented only by the Fe-depleted variety, though also with complex compositional variations (Figs 15, 16).

Trace and rare earth element (RRE) geochemistry of siderite. — Disseminated siderite cement is enriched in trace elements, compared to concretionary sid-
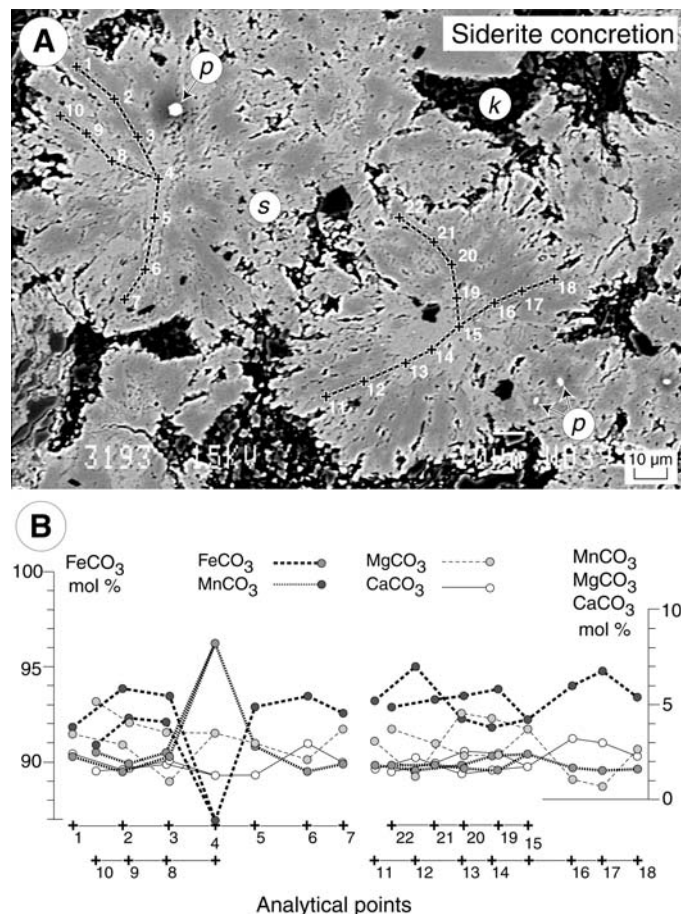
Fig. 14. Compositional changes in spherulitic siderite forming concretions in the sideritic horizon III. BEI image (**A**) of siderite spherules (s) embedding microgranular pyrite (p). Kaolinite (k) occurs in inter-particle pore space. 1 to 22 are analytical points along EDS quantitative compositional profile shown in **B**.

erite present in the same sedimentary horizons (Table 1). This enrichment is particularly pronounced for Zn and Sr (Fig. 17). It is also evident for Ni, V, Mo, and Cu. The patterns of Cr, Co, U, and Th are less clear, though with a general, slight enrichment trend in the cement. This trend is matched by a similar enrichment with REEs and yttrium.

Isotopic composition of carbon and oxygen in siderite. — Siderite forming concretions has $\delta^{13}C$ values between +1 and +8‰, without any clear difference between the sideritic horizons (Table 2, Fig. 18). Disseminated siderite cement has negative values varying between -4.5 and -1.5‰. There is no noticeable difference in the $\delta^{18}O$ values between these two siderite types (Table 2). These values are strongly negative, fluctuating between -20 and -15‰.
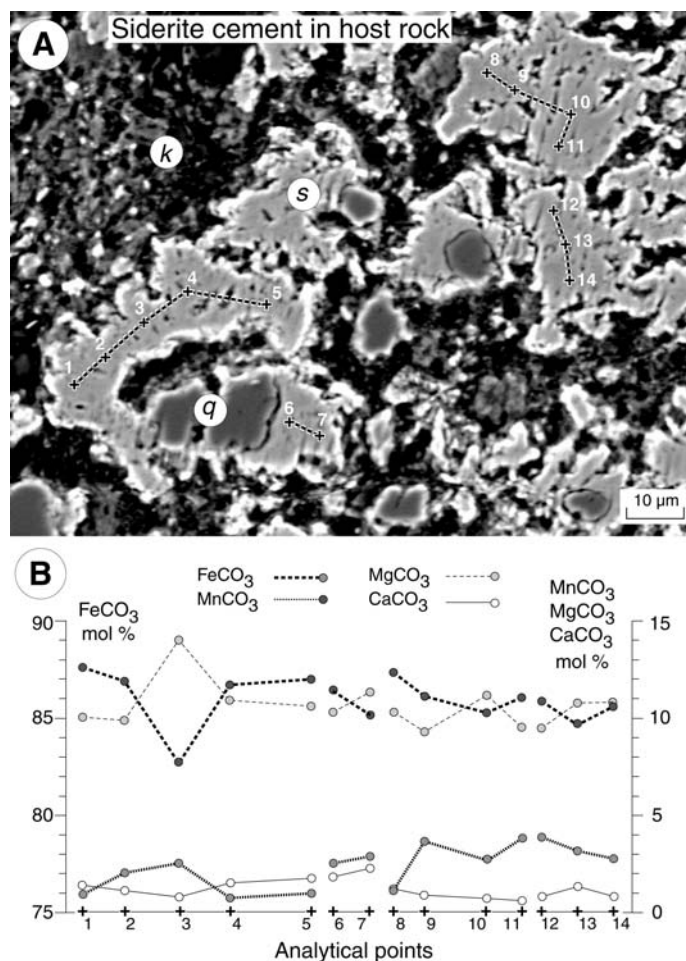
Fig. 15. Compositional changes in disseminated siderite cement in host rock of the sideritic horizon I. BEI image (**A**) of siderite aggregates and coatings (s) around detrital quartz grains (q). Kaolinite (k) occurs in rock matrix. 1 to 14 are analytical points along EDS quantitative compositional profile shown in **B**.

Isotopic composition of strontium in siderite. — There is no discernible trend in the isotopic composition of strontium between the concretions and the disseminated cement (Table 3). The obtained values ($^{87}Sr/^{86}Sr$ between 0.7271 and 0.7281) suggest that the dominant supply of strontium was from the weathering environment of the crystalline rock basement.

Discussion

The petrographic, geochemical, and isotopic data presented in this paper indicate that siderite in the Panorama Point Beds represents a sequence of early
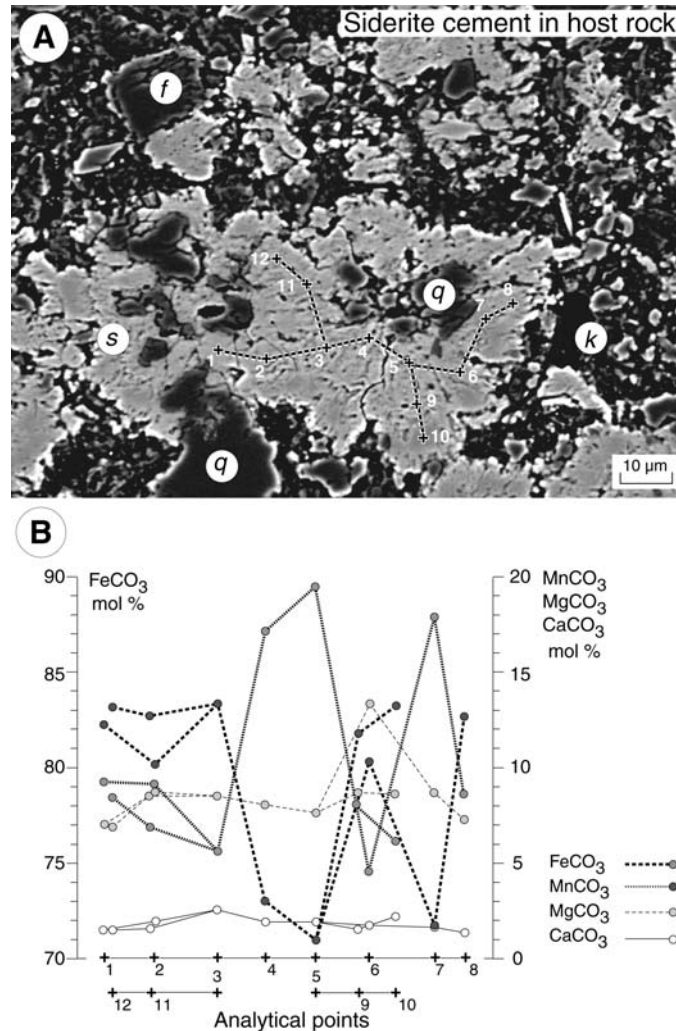
Fig. 16. Compositional changes in disseminated siderite cement in host rock of the sideritic horizon III. BEI image (**A**) of siderite aggregates and coatings (s) around detrital quartz grains (q). Detrital feldspar (f) and kaolinite (k) occur in rock matrix. 1 to 12 are analytical points along EDS quantitative compositional profile shown in **B**.

diagenetic precipitates formed in fresh-water environments of the Lambert Graben depositional system. The recognition and characterization of this sequence allows for reconstruction of biogeochemical processes related to sedimentary transformations and mineralization of organic matter (Fig. 19). The typical diagenetic sequence in an organic-rich, fresh-water sediment column is defined by dominant microbiological processes involved in decomposition of organic matter (Coleman 1985; Curtis 1987; Canfield 1994). It includes a surficial oxic zone, in which free oxygen is the overwhelming oxidant. This zone is underlain by a suboxic zone, in

Table 1

Contents of trace and rare earth elements and yttrium (ppm) in concretionary siderite (C-samples) and in disseminated siderite cement (H-samples).

Sample	Ni	Cr	V	Mo	Zn	Cu	Co	Cd	Sr	Pb	Ba	U	Th	Re	Pt	Pd	Al
C1	96	96	153	28	251	106	59	17	116	53	427	19	160	8	9	25	12413
H1	251	229	232	63	778	362	64	23	399	102	1449	25	538	20	20	29	33559
C2	152	134	147	9	249	72	18	6	120	67	626	7	129	2	2	9	14630
H2	150	144	180	9	365	140	46	8	224	76	288	10	248	3	3	6	19164
C3	60	40	66	2	147	26	22	2	97	13	385	2	42	1	0	4	6641
H3	251	115	190	2	410	92	37	3	133	37	225	4	113	2	0	5	15183

Sample	La	Ce	Pr	Nd	Sm	Eu	Gd	Tb	Dy	Ho	Er	Tm	Yb	Lu	ΣREE		Y
C1	5.2	9.3	1.4	3.2	2.7	1.4	3.7	0.4	3.0	0.4	2.2	0.2	2.1	0.2	35.4		10.6
H1	13.2	25.8	3.0	9.4	5.2	1.4	8.0	0.4	5.5	0.4	3.1	0.3	2.8	0.2	78.7		20.8
C2	2.8	5.3	0.6	1.5	1.4	0.5	2.3	0.1	1.8	0.1	1.2	0.1	1.7	0.0	19.4		8.2
H2	4.3	8.4	0.9	4.9	1.5	0.4	2.4	0.1	2.3	0.1	1.6	0.1	1.3	0.1	28.4		11.1
C3	1.8	3.2	0.3	0.9	0.6	0.2	1.1	0.1	1.0	0.1	0.7	0.0	0.7	0.0	10.7		5.8
H3	4.2	8.5	0.9	1.9	1.5	0.4	2.5	0.1	1.9	0.1	1.2	0.0	1.2	0.0	24.4		9.1

which major oxidation reactions involve bacterial reduction of manganese and iron. The zone of bacterial sulphate reduction is not clearly defined or absent in the fresh-water sequence. Instead, the anoxic methanic zone dominates the underlying subsurface environment due to ubiquitous bacterial fermentation processes.

The analyzed material strongly suggests the existence of two stages of siderite precipitation in the diagenetic sequence of the Panorama Point Beds: (1) early precipitation of disseminated cement that preceded (2) localized precipitation of cement to form concretionary bodies. The two processes occurred very early after sediment accumulation, as indicated by the microscopic features of siderite and the uncompacted nature of concretionary matrices.

Noticeable substitutions of magnesium for iron in the disseminated cement, coupled with the negative $\delta^{13}C$ values and enrichment in trace and rare earth elements, suggest nearsurface formation of siderite in a suboxic environment dominated by microbial reduction of iron and oxidative degradation of sedimentary organic matter. Substitutions of Mn^{2+} for Fe^{2+} in the siderite cement record also microbial reduction of manganese. The common development of disseminated siderite in the Panorama Point Beds suggests maintenance of a delicate balance between production and burial of organic matter and a supply of reactive iron and manganese. This may indicate an extended vegetation in the swamp to stagnant water environments of the early Lambert valley and an excess supply of oxidants from the crystalline highlands. It is consistent with the petrographic composition of the clastic sediments and the preserved carbonaceous material and palynomorphs.

Table 2

Isotopic composition of carbon (δ^{13}C) and oxygen (δ^{18}O) in concretionary siderite (C-samples) and in disseminated siderite cement (H-samples).

Siderite concretions			Siderite cement in host rock		
Sample	δ^{13}C (‰ VPDB)	δ^{18}O (‰ VPDB)	Sample	δ^{13}C (‰ VPDB)	δ^{18}O (‰ VPDB)
I sideritic horizon					
C1-1	1.16	-17.34	H1-1	-1.93	-17.22
C1-2	2.90	-18.69	H1-2	-4.40	-20.38
C1-3	3.40	-18.19			
C1-4	5.00	-17.49			
C1-5	5.50	-17.49			
C1-6	5.78	-16.20			
II sideritic horizon					
C2-1	3.89	-17.06	H2-1	-2.01	-17.56
C2-2	3.67	-16.79	H2-2	-1.70	-19.59
C2-3	5.70	-17.79	H2-3	-3.15	-15.65
C2-4	5.14	-18.27	H2-4	-1.90	-18.29
C2-5	2.41	-19.12	H2-5	-3.73	-15.37
C2-6	7.88	-17.49	H2-6	-3.81	-16.87
C2-7	3.95	-18.41			
III sideritic horizon					
C3-1	4.21	-14.81	H3-1	-1.89	-15.82
C3-2	3.93	-14.67	H3-2	-2.20	-17.79
C3-3	4.72	-14.64	H3-3	-3.99	-16.34
C3-4	3.68	-15.47	H3-4	-2.98	-16.31
C3-5	3.34	-15.83	H3-5	-1.59	-17.01
C3-6	3.63	-15.41	H3-6	-1.50	-18.23
mC3-7	2.62	-14.67	H3-7	-1.50	-17.99
C3-8	2.06	-15.02			
C3-9	3.24	-15.85			
C1-7	7.96	-15.29			

Table 3

Isotopic composition of strontium (^{87}Sr/^{86}Sr) in concretionary siderite (C-samples) and in disseminated siderite cement (H-samples).

	Siderite concretion			Siderite cement in host rock		
	Sample	^{87}Sr/^{86}Sr	error in %	Sample	^{87}Sr/^{86}Sr	error in %
I sideritic horizon	C1	0.727575	± 0.0024	H1	0.727442	± 0.0016
II sideritic horizon	C2	0.727283	± 0.0011	H2	0.728106	± 0.0028
III sideritic horizon	C3	0.725784	± 0.0017	H3	0.727078	± 0.0019
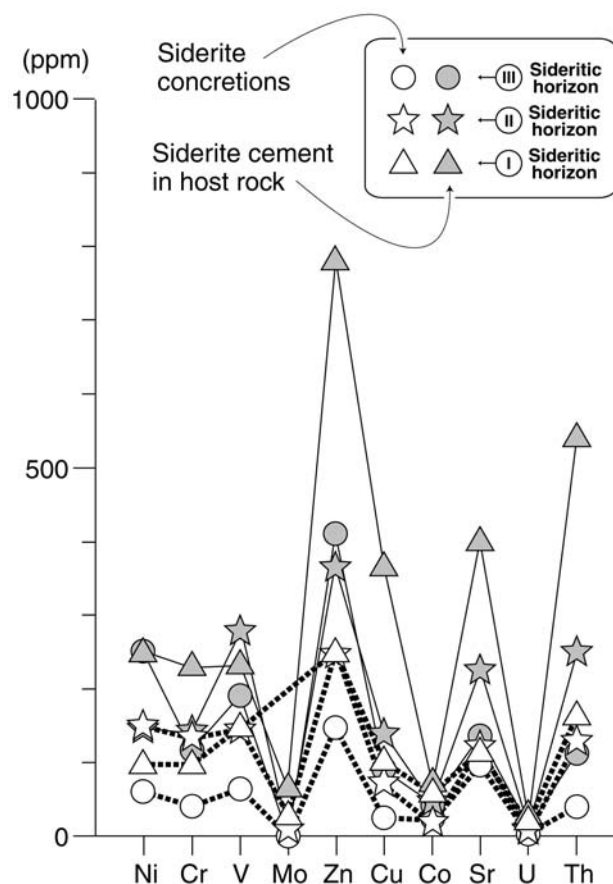
Fig. 17. Changes in the content of trace elements (Ni, Cr, V, Mo, Zn, Cu, Co, Sr, U, Th) in concretionary siderite and in disseminated siderite cement.

A noticeable increase in the content of manganese in disseminated siderite of the upper upward-coarsening cycle indicates changes in the supply of reactive manganese during the depositional history of the succession.

Negligible amounts of authigenic pyrite in the Panorama Point Beds suggest very limited bacterial sulphate reduction in the subsurface, owing most probably to a general lack of dissolved sulphate in the surficial and pore waters. This is consistent with a fresh-water depositional system in the Lambert Graben, which was reinforced by meteoric input on the surrounding highlands. Strongly negative values of the $\delta^{18}O$ of siderite support this interpretation. Pyrite microgranules are not evident within siderite clusters in the disseminated cement, but they are always found inside siderite spherules in concretions. This supports the interpretation that the disseminated cement precipitated in the nearsurface suboxic environment prior to bacterial sulphate reduction. It also suggests that the development of concretionary bodies post-dated the limited bacterial sulphate reduction in the sediment. The positive $\delta^{13}C$
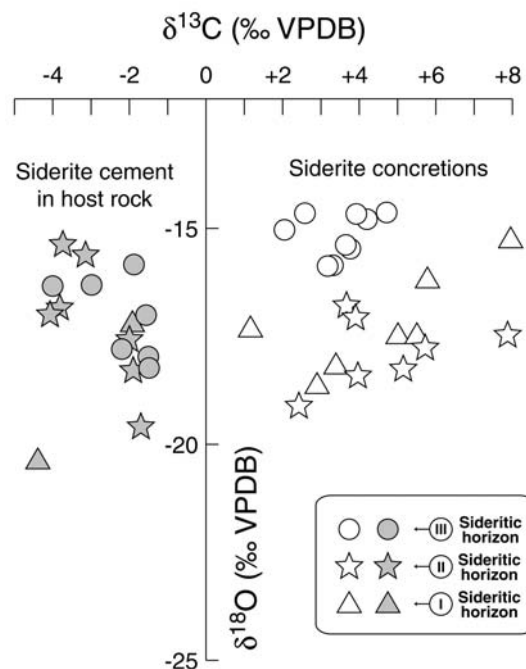
Fig. 18. Plot of $\delta^{13}C$ and $\delta^{18}O$ values of concretionary siderite and disseminated siderite cement.

values of concretionary siderite point to methanogenic fermentation processes in the subsurface. The obtained values record mixtures of two types of siderite, in which the earlier one precipitated in a suboxic environment, and should have negative $\delta^{13}C$ values. It is, therefore, likely that the later generation of siderite forming the concretionary bodies, attributed here to the anoxic methanic environment, should have correspondingly more positive values.

The concretions reflect localized precipitation of siderite at numerous nucleation sites that showed a general horizontal alignment in the sediment column. This suggests that their distribution in the sequence reflects episodes of enhanced supply of carbonate generated in the anoxic methanic environment as well as ferrous iron to particluar levels of the subsurface environment. Enhanced formation of the concretions in the muddy sediment that was rapidly buried due to progradation of sandy channel facies is a likely scenario, though evidence of this relationship is circumstantial. The actual depth in the sediment column at which the concretions grew is difficult to estimate, but a few metres at most below the sediment surface is likely. The dominant ovoid and lensoid shapes of the concretions imply no insignificant difference in permeability of the sediment in vertical and horizontal directions, supporting shallow formation. Rapid change of structure and fabric at the margins of the concretions, which become more clastic and mechanically oriented, suggests that the growth of concretions terminated prior to final cementation of the succession.
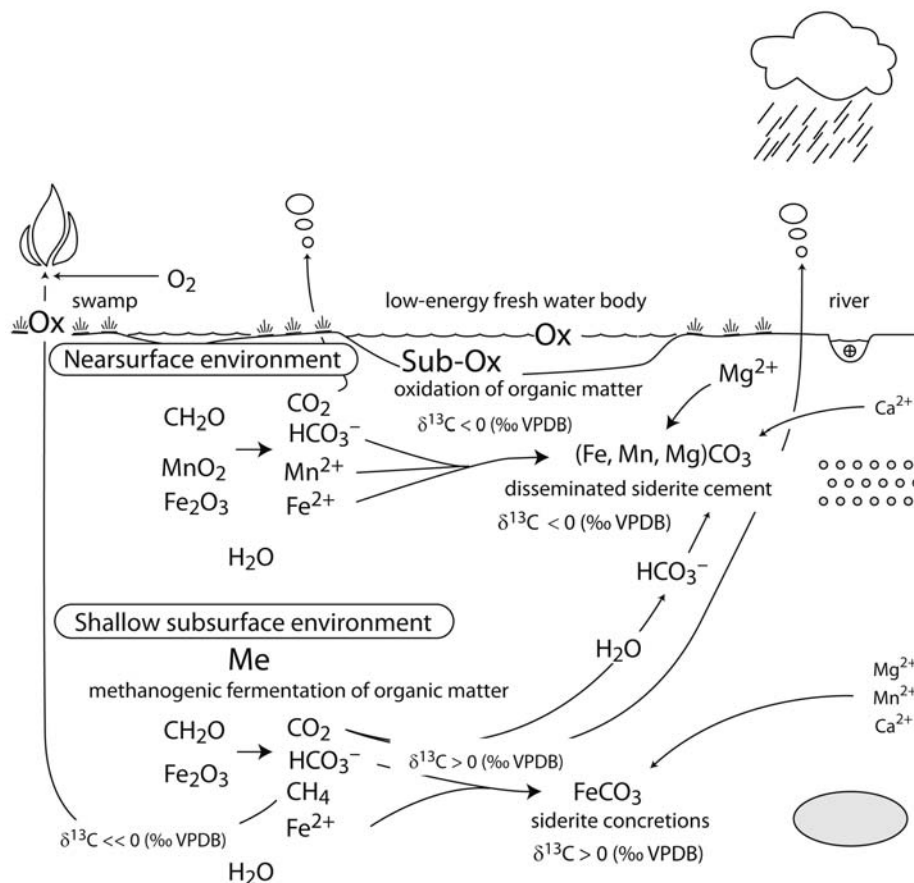
Fig. 19. Model of depositional to early diagenetic system of the Panorama Point Beds showing biogeochemical regimes of siderite formation in fresh-water environment of the southern Gondwana. Ox – oxic environment; Sub-Ox – suboxic environment; Me – anoxic methanic environment.

Termination of the deposition of Panorama Point Beds was associated with a slight uplift of this part of the Lambert Graben and partial erosion of sediments. This may well explain a change in early diagenetic regime due to an event with unfavourable conditions for deposition of organic matter. Corrosional margins of sideritic spherules and rims of goethite observed both in the disseminated siderite cement and in concretions suggest infiltration of oxygenated waters into the porous clastic strata during this event. The final cement in the Panorama Point Beds is vermicular kaolinite, which owes its origin to burial diagenesis of the clastic facies.

During the formation of the Lambert Graben and deposition of the Radok Conglomerate, MacRobertson Land was located within the Polar circle on Gondwana (Powell and Li 1994). This region is supposed to have been covered by massive ice sheets during the Carboniferous and Early Permian (Scotese 1997; Zeigler *et al.* 1997; Scotese *et al.* 1999). However, the lack of glacial deposits in the present-day

outcrop in the Prince Charles Mts, coupled with common occurrence of biogenic siderite and carbonized flora remnants in the Radok Conglomerate, may suggest that the ice sheets in East Antarctica were less massive and extensive than previously hypothesized or they disappeared before the fluvial system of the Lambert Graben had formed. The fluvial valley of the Lambert Graben was likely to be at least 1000 km long, draining huge areas located southwards (Fedorov *et al.* 1982; Mikhalsky *et al.* 2001). The Upper Paleozoic outcrops known in the Transantarctic Mountains (TAM), including Victoria Land, the Darwin Glacier region, and the central TAM, are located at distances of about 2000 km (Fig. 1). They indicate the absence of massive ice cover during the Carboniferous and sedimentation in ice-marginal to periglacial settings during the Permian (Isbell *et al.* 1997, 2001, 2003).

Conclusions

Siderite is common in the Panorama Point Beds of the Radok Conglomerate (Early to Middle Permian), which is the oldest known sedimentary unit in the Prince Charles Mountains, MacRobertson Land, East Antarctica. This siderite records biogeochemical processes related to sedimentary transformations and mineralization of organic matter in the depositional system of the early stage of development of the Lambert Graben, a major structural valley in the southern part of Gondwana. There are two types of siderite, which correspond to the two consequent early diagenetic environments in the fresh-water clastic facies: (1) siderite cement that occurs throughout the sedimentary succession of the Panorama Point Beds, reflecting disseminated precipitation in a nearsurface environment dominated by oxidation of organic matter and reduction of iron and manganese; (2) siderite concretions that occur in three superimposed muddy horizons, reflecting localized precipitation in a subsurface environment dominated by methanogenic fermentation of organic matter and reduction of iron. These two siderite types show differences in their chemical and carbon isotopic composition. Disseminated cement is composed of Fe-depleted siderite with elevated content of magnesium, and trace and rare earth elements; and it has negative $\delta^{13}C$ values. Concretionary bodies embrace relatively pure siderite with positive $\delta^{13}C$ values. There are no noticeable differences in the oxygen and strontium isotopic compositions between the siderite types. These characters reflect a common origin in a fresh-water depositional system reinforced by meteoric input and drainage of crystalline highlands surrounding the Lambert Graben.

The common presence of siderite in the Panorama Point Beds suggests that fresh-water environments of the Lambert Graben received an abundant supply of detrital plant matter starting from the early history of its development. The lack of glacial deposits in the area, coupled with thin coaly laminae even in the oldest clastic sediments, suggests that the beds were deposited later than the main pulse of Gondwanan glaciation.

References

ALEKSASHIN N.D. and LAIBA A.A. 1993. Stratigraphy and lithofacial features of Permian sedimentary sequence of the Beaver Lake western coast (the Prince Charles Mountains, East Antarctica). *The Antarctic, Russiant Committee on Antarctic Research Report* 31: 43–51 (in Russian).

CANFIELD D.E. 1994. Factors influencing organic carbon preservation in marine sediments. *Chemical Geology* 114: 315–329. http://dx.doi.org/10.1016/0009-2541(94)90061-2

CANTRILL D.J., DRINNAN A.N. and WEBB J.A. 1995. Late Triassic plant fossils from the Prince Charles Mountains, East Antarctica. *Antarctic Science* 7: 51–62.
http://dx.doi.org/10.1017/S0954102095000095

CAROTHERS W.W., ADAMI L.H. and ROSENBAUER R.J. 1988. Experimental oxygen isotope fractionation between siderite-water and phosphoric acid liberated CO_2-siderite. *Geochimica et Cosmochimica Acta* 52: 2445–2450. http://dx.doi.org/10.1016/0016-7037(88)90302-X

CÚNEO N.R. 1996. Permian phytogeography in Gondwana. *Palaeogeography Palaeoclimatology Palaeoecology* 125: 75–104. http://dx.doi.org/10.1016/S0031-0182(96)00025-9

COLEMAN M.L. 1985. Geochemistry of diagenetic non-silicate minerals: kinetic considerations. *Philosophical Transactions of the Royal Society London* A315: 39–56.
http://dx.doi.org/10.1098/rsta.1985.0028

CURTIS C.D. 1987. Inorganic geochemistry and petroleum exploration. *In*: J. Brooks and D. Welte (eds) *Advances in Petroleum Geochemistry*, 2. Academic Press, London: 91–140.

DIBNER A.F. 1976. Late Permian palynofloras from sedimentary rocks from the Beaver Lake area, Esat Antarctica. *The Antarctic, Soviet Committee on Antarctic Research, Report* 15: 41–52 (in Russian).

DICKMANN B. and WOPFNER H. 1996. Petrographic and diagenetic signatures of climatic change in peri- and postglacial Karoo Sediments of SW Tanzania. *Palaeogeography Palaeoclimatology Palaeoecology* 125: 5–25. http://dx.doi.org/10.1016/0031-0182(95)00084-4

DIMICHELE W.A., PFEFFERKORN H.W. and PHILLIPS T.L. 1996. Persistence of Late Carboniferous tropical vegetation during glacially driven climatic and sea-level fluctuations. *Palaeogeography Palaeoclimatology Palaeoecology* 125: 105–128.
http://dx.doi.org/10.1016/S0031-0182(96)00026-0

DOS SANTOS P.R., ROCHA-CAMPOS A.C. and CANUTO J.R. 1996. Patterns of late Paleozoic deglaciation in the Parana Basin, Brazil. *Palaeogeography Palaeoclimatology Palaeoecology* 125: 165–184. http://dx.doi.org/10.1016/S0031-0182(96)00029-6

FAURE K. and COLE D. 1999. Geochemical evidence for lacustrine microbial blooms in the vast Permian Main Karoo, Parana, Falkland Islands and Huab basins of southwestern Gondwana. *Palaeogeography Palaeoclimatology Palaeoecology* 152: 189–213.
http://dx.doi.org/10.1016/S0031-0182(99)00062-0

FEDOROV L.V., GRIKUROV G.E., KURININ R.G. and MASLOV V.N. 1982. Crustal structure of the Lambert Glacier area from geophysical data. *In*: C. Craddock (ed.) *Antarctic Geoscience*. University of Wisconsin Press, Madison: 931–936.

FIELDING C.R. and WEBB J.A. 1995. Sedimentology of the Permian Radok Conglomerate in the Beaver Lake area of Mac.Robertson Land, East Antarctica. *Geological Magazine* 132: 51–63. http://dx.doi.org/10.1017/S0016756800011420

FIELDING C.R. and WEBB J.A. 1996. Facies and cyclicity of the Late Permian Bainmedart Coal Measures in the Northern Prince Charles Mountains, MacRobertson Land, Antarctica. *Sedimentology* 43: 295–322. http://dx.doi.org/10.1046/j.1365-3091.1996.d01-6.x

FOLK R.L. 1974. *Petrology of Sedimentary Rocks*. Hemphill Publishing Company, Austin, Texas; 184 pp.

GONZALEZ C.R. 1990. Development of the Late Paleozoic glaciations of the South American Gondwana in western Argentina. *Palaeogeography Palaeoclimatology Palaeoecology* 79: 275–287. http://dx.doi.org/10.1016/0031-0182(90)90022-Y

GOULD K.W. and SMITH J.W. 1979. The genesis and isotopic composition of carbonates associated with some Permian Australian coals. *Sedimentary Geology* 24: 137–150.

HARROWFIELD M., HOLDGATE G., WILSON C. and MCLOUGHLIN S. 2005. Tectonic significance of the Lambert Graben, East Antarctica: reconstructing the Gondwanan rift. *Geology* 33: 197–200. http://dx.doi.org/10.1130/G21081.1

ISBELL J.L. and CÚENO N.R. 1996. Depositional framework of Permian coal-bearing strata, southern Victoria Land, Antarctica. *Palaeogeography Palaeoclimatology Palaeoecology* 125: 217–238. http://dx.doi.org/10.1016/S0031-0182(96)00032-6

ISBELL J.L., GELHAR G.A. and SEEGERS G.M. 1997. Reconstruction of preglacial topography using a postglacial flooding surface: Upper Paleozoic deposits, central Transantarctic Mountains, Antarctica. *Journal of Sedimentary Research* 67: 264–273.

ISBELL J.L., MILLER M.F., BABCOCK L.E. and HASIOTIS S.T. 2001. Ice-marginal environment and ecosystem prior to initial advance of the late Paleozoic ice sheet in the Mount Butters area of the central Transantarctic Mountains, Antarctica. *Sedimentology* 48: 953–970. http://dx.doi.org/10.1046/j.1365-3091.2001.00403.x

ISBELL J.L., LENAKER P.A., ASKIN R.A., MILLER M.F. and BABCOCK L.E. 2003. Reevaluation of the timing and extent of late Paleozoic glaciation in Gondwana: Role of the Transantarctic Mountains. *Geology* 31: 977–980. http://dx.doi.org/10.1130/G19810.1

KEMP E.M. 1973. Permian flora from the Beaver Lake area, Prince Charles Mountains, Antarctica. I. Palynological examination of samples. *Bulletin of the Bureau of Mineral Resources, Geology and Geophysics, Australia* 126: 7–12.

KETZER J.M., HOLZ M., MORAD S. and AL-AASM I.S. 2003. Sequence stratigraphic distribution of diagenetic alterations in coal-bearing, paralic sandstones: evidence from the Rio Bonito Formation (early Permian), southern Brazil. *Sedimentology* 50: 855–877. http://dx.doi.org/10.1046/j.1365-3091.2003.00586.x

LINDSTRÖM S. and MCLOUGHLIN S. 2007. Synchronous palynofloristic extinction and recovery after the end-Permian event in the Prince Charles Mountains, Antarctica: implications for palynofloristic turnover across Gondwana. *Review of Palaeobotany and Palynology* 145: 89–122. http://dx.doi.org/10.1016/j.revpalbo.2006.09.002

MCKELVEY B.C. and STEPHENSON N.C.N. 1990. A geological reconnaissance of the Radok Lake area, Amery Oasis, Prince Charles Mountains. *Antarctic Science* 2: 53–66. http://dx.doi.org/10.1017/S0954102090000062

MCLOUGHLIN S. and DRINNAN A.N. 1997a. Revised stratigraphy of the Permian Bainmedart Coal Measures, northern Prince Charles Mountains, East Antarctica. *Geological Magazine* 134: 335–353. http://dx.doi.org/10.1017/S0016756897006870

MCLOUGHLIN S. and DRINNAN A.N. 1997b. Fluvial sedimentology and revised stratigraphy of the Triassic Flagstone Bench Formation, northern Prince Charles Mountains, East Antarctica. *Geological Magazine* 134: 781-806. http://dx.doi.org/10.1017/S0016756897007528

MCLOUGHLIN S., LINDSTRÖM S. and DRINNAN A.N. 1997. Gondwana floristic and sedimentological trends during the Permian–Triassic transition: new ewidence from the Amery Group, northern Princes Charles Mountains, East Antarctica. *Antarctic Science* 9: 281–298. http://dx.doi.org/10.1017/S0954102097000370

MIKHALSKY E.V., SHERATON J.W., LAIBA A.A., TINGEY R.J., THORST D.E., KAMENEV E.N. and FEDOROV L.V. 2001. Geology of the Prince Charles Mountains, Antarctica. *AGSO – Geoscience Australia Bulletin* 247: 209 pp.

MISHIRA H.K. 1996. Comparative petrological analysis between the Permian coals of India and Western Australia: paleoenvironments and thermal history. *Palaeogeography Palaeoclimatology Palaeoecology* 125: 199–216. http://dx.doi.org/10.1016/S0031-0182(96)00031-4

MOND A. 1972. Permian sediments of the Beaver Lake area, Prince Charles Mountains. *In*: R.J. Adie (ed.) *Antarctic Geology and Geophysics*. Universitetsforlaget, Oslo: 585–589.

POWELL C.M. and LI Z.X. 1994. Reconstruction of the Panthalassan margin of Gondwanaland . *In*: J.J. Veevers and C.M. Powell (eds) Permian–Triassic Pangean Basins and Foldbelts along the Panthalassan margin of Gondwanaland. *Geological Society of America Memoir* 184: 5–9.

RAVICH G.M. 1974. The cross-section of Permian coal-bearing strata in the Beaver Lake area (Prince Charles Mountains, East Antarctica). *The Antarctic, Soviet Committee on Antarctic Research Report* 13: 19–35 (in Russian).

SCOTESE C.R. 1997. *The PALEOMAP Project: Paleogeographic Atlas and Plate Tectonic Software*. University of Texas, Department of Geology, Austin, Texas.

SCOTESE C.R., BOUCOT A.J. and MCKERROW W.S. 1999. Gondwanan palaeogeography and palaeoclimatology. *Journal of African Earth Sciences* 28: 99–114. http://dx.doi.org/10.1016/S0899-5362(98)00084-0

UYSAL I.T., GOLDING S.D. and GLIKSON M. 2000. Petrographic and isotope constraints on the origin of authigenic carbonate minerals and the associated fluid evolution in Late Permian coal measures, Bowen Basin (Queensland), Australia. *Sedimentary Geology* 136: 189–206. http://dx.doi.org/10.1016/S0037-0738(00)00097-X

WEBB J.A. and FIELDING C.R. 1993a. Permo-Triassic sedimentation within the Lambert Graben, northern Prince Charles Mountains, East Antarctica. *In*: R.H. Findlay, R. Unrug, M.R. Banks and J.J. Veevers (eds) *Gondwana Eight: Assembly, Evolution and Dispersal*. A. Balkema, Rotterdam: 357–369.

WEBB J.A. and FIELDING C.R. 1993b. Revised stratigraphical nomenclature for the Permo-Triassic Flagstone Bench Formation, northern Prince Charles Mountains, East Antarctica. *Antarctic Science* 5: 409–410. http://dx.doi.org/10.1017/S0954102093000549

WHITE M.E. 1969. Permian flora from the Beaver Lake area, Prince Charles Mountains, Antarctica. 2: Plant fossils. *Bureau of Mineral Resources, Australia, Bulletin* 126: 13–18.

YEMANE K. and KELTS K. 1996. Isotope geochemistry of Upper Permian early diagenetic calcite concretions: Implications for Late Permian waters and surface temperatures in continental Gondwana. *Palaeogeography Palaeoclimatology Palaeoecology* 125: 51–73. http://dx.doi.org/10.1016/S0031-0182(96)00024-7

ZIEGLER A.M., HULVER M.L. and ROWLEY D.B. 1997. Permian world topography and climate. *In*: I.P. Martini *et al.* (eds) *Late Glacial and Postglacial Environmental Changes: Quaternary, Carboniferous–Permian, and Proterozoic*. Oxford University Press, Oxford: 111–146.